DOI 10.1007/s11223-020-00189-4
Strength of Materials, Vol. 52, No. 3, May, 2020

STATIC CRACK RESISTANCE OF HEAT-RESISTANT KhN43MBTYu NICKEL-CHROMIUM ALLOY IN GASEOUS HYDROGEN

O. I. Balyts'kyi,[a,b,1] L. M. Ivas'kevych,[a,2] and J. J. Eliasz[b,3]

UDC 620.197:669.788

The effect of hydrogen at a pressure of up to 35 MPa and a content of up to 29 ppm on the strength, ductility, short-term and long-term static crack resistance of four KhN43MBTYu (EP-915VD) alloy modifications with different heat treatment modes and chemical composition has been studied. It has been found that the critical stress intensity factor K_{Ic} in the presence of hydrogen, just as the ductility characteristics of smooth specimens, depends on the deformation rate, reaching minimum values at rates of less than 0.1 mm/min. The fracture toughness decreases under the action of hydrogen by a factor of 2.5, and the plane strain state occurs at a much smaller specimen thickness. An optimal combination of high strength, ductility, short- and long-term static crack resistance in air and hydrogen has been achieved in a fine-grained alloy with low carbon and sulfur content. Based on the results of long-term static crack resistance tests at the predetermined maximum fatigue test duration of 300 h, the invariant characteristics of crack resistance, the threshold values of stress intensity factor in hydrogen, have been determined, which vary from 23 to 48 MPa $\cdot m^{1/2}$ depending on the alloy heat treatment mode.

Keywords: carbides, intermetallics, short-term and long-term static crack resistance, hydrogen brittleness, heat-resistant nickel alloy.

Introduction. The critical stress intensity factor (SIF) K_{Ic} under short-term load and the threshold SIF value K_{ISCC} (K_{IHST} in hydrogen) under the long action of an aggressive environment are important characteristics of structural materials, which are used to assess the reliability and life of engineering structures if the part has technological or service-induced cracks [1–6]. The experimental determination of these parameters in gaseous hydrogen is complicated by the fact that to ensure self-similarity conditions in the case of ductile and slightly crack and notch sensitive hydrogen-resistant steels and alloys, large specimens must be used [1–5]. Therefore, the hydrogen brittleness of materials in gaseous hydrogen at high pressure was generally assessed from the results of short-term strength and low-cycle life tests [1, 2, 7–10]. The existing equipment [11] allows one to determine the crack resistance parameters and permissible operating conditions of materials.

Three main parameters play an important role in hydrogen embrittlement: (i) hydrogen content and condition, (ii) the chemical composition and structural state of the alloy after heat treatment, and (iii) the value of stresses (induced by internal or external service loads) in the workpiece. Changing the chemical composition and structure of the alloy determines largely its strength, ductility and fracture toughness and hence affects hydrogen embrittlement susceptibility. Dopants change the phase composition and structure, affect the grain size, and accelerate or inhibit the

[a]Karpenko Physico-Mechanical Institute, National Academy of Sciences of Ukraine, Lviv, Ukraine ([1]balitskii@ipm.lviv.ua; [2]ivaskevich@ipm.lviv.ua). [b]West Pomeranian University of Technology in Szczecin, Szczecin, Poland ([3]Jacek.Eliasz@zut.edu.pl). Translated from Problemy Prochnosti, No. 3, pp. 61 – 74, May – June, 2020. Original article submitted April 15, 2019.

TABLE 1. Chemical Composition (wt.%) of Alloy Modifications under Study

Chemical composition	C	Cr	Fe	Mo	Ti	Al	V	Mn	Si	S	P	Others
CCI	0.05	14.5	36.58	1.75	1.67	0.10	0.3	0.10	0.18	0.005	0.008	Nb2.70 Ca0.02 Cu0.02 Zr0.02
CCII	0.03	14.1	36.06	1.48	1.81	0.28	0.1	0.07	0.10	0.001	0.006	Nb2.55 Ca0.02 Cu0.02 Zr0.02

TABLE 2. Heat Treatment Mode and Grain Size

No.	Chemical composition	Heat treatment mode	d, μm
1	CCI	Hardening at 1300 K, 2h, air; aging at 1023 K, 8h + 923 K, 8h, air (HTI)	27
2	CCII	Hardening at 1300 K, 2h, air; aging at 1023 K, 8h + 923 K, 8h, air (HTI)	27
3	CCII	After HTI, soldering simulation at 1473 K, 15 min + 1273 K, 2h, air (HTII)	190
4	CCII	After HTII, aging at 1023 K, 8h + 923 K, 8h, air (HTIII)	190

crack initiation and propagation. Therefore, to ensure the reliable operation of products made of the alloy and to increase the brittle fracture resistance in a hydrogen environment, it is necessary to select its chemical composition and heat treatment mode such that they provide a structural state with high fracture toughness values.

The aim of the work is to study the effect of high-pressure gaseous hydrogen on the short-term and long-term static crack resistance of KhN43MBTYu (EP-915VD) nickel alloy modifications with different chemical composition and heat treatment modes.

Material and Research Procedure. According to the results of previous research, the KhN43MBTYu alloy has a high strength, ductility and hydrogen resistance in a wide temperature range [10–12]. It is a nickel- and iron-based multicomponent gamma solid solution. Tables 1 and 2 present two chemical compositions (CC) and three modes of heat treatment (HT) of the alloy. The main difference between CCI and CCII is a low carbon and sulfur content. Both modifications are doped with copper, which enhances the hydrogen resistance of precipitation-hardened heat-resistant nickel alloys, and this changes their electron density, surface condition, and the rate of hydrogen penetration from the gaseous environment [12]. Zirconium in nickel-iron alloys facilitates the spheronization of secondary grain boundary phases, which increases long-term strength [13] and hydrogen resistance [11, 14]. The percentage of the main strengthening phase, $(Ni, Cr, Fe)_3(Nb, Al, Ti, Mo)$ intermetallic, was determined by physicochemical phase analysis in an aqueous electrolyte with ammonium sulfate and the percentage of carbides (mainly $Me_{23}C_6$) in a methanol-based electrolyte.

The KhN43MBTYu alloy is a nickel- and iron-based multicomponent γ-solid solution, in which an intermetallic strengtnening phase and carbides precipitate. After vacuum arc remelting, it has a different chemical composition (CCI, CCII), but its microstructure resulting from HTI is the same (Fig. 1a). The mean grain size d = 27 μm. The percentage of the γ' phase and carbides is 10 and 1.5 wt.% (CCI) and 10 and 1.0 wt.% (CCII). After HTII in soldering simulation mode at 1473 K, a significant growth of grains, whose mean size is 190 μm (Table 2), and alloy depletion of excess and strengthening phases are observed (Fig. 1b). The percentage of the γ' phase and carbides is 6 and 0.5 wt.%, respectively. At the grain boundaries, there are only γ' phase precipitates. Additional double aging at 1023 K, 8 h and at 923 K, 8 h in air after soldering simulation (HTIII) results in a higher percentage of dispersed phases, especially at the grain boundaries. In this case, the mean grain size does not change and reaches 190 μm (Fig. 1c). The percentage of the γ' phase and carbides is 14 and 1.0 wt.%.

TABLE 3. Strength, Ductility, and Crack Resistance Characteristics of Alloy Modifications at Room Temperature and an Extension Rate of 0.1 mm/min

No. (Table 2)	γ′ phase content (wt.%)	Percentage of carbides (wt.%)	Hydrogen content C_H, ppm	σ_u, MPa	$\sigma_{0.2}$, MPa	δ, %	ψ, %	K_{Jc}, MPa · m$^{1/2}$ (air)	K_c, MPa · m$^{1/2}$	β_ψ	β_{Kc}
1	10	1.5	19	1160 / 960	780 / 740	25 / 4	38 / 14	143	121 / 52	0.37	0.36
2	10	1	21	1250 / 1120	820 / 780	29 / 7	49 / 21	154	130 / 63	0.43	0.41
3	6	0.5	13	820 / 790	510 / 500	37 / 34	38 / 36	91	83 / 80	0.95	0.88
4	14	1	18	1180 / 940	770 / 780	21 / 3	23 / 9	73	74 / 30	0.39	0.41

Note. $\beta_\psi = \psi_H / \psi_{He}$, $\beta_{Kc} = K_{cH} / K_{Ic}(J)$; above the line are hydrogen-uncharged specimens with a thickness of 20 mm in air, and below the line are specimens hydrogen-charged in mode 1 in hydrogen at a pressure of 35 MPa.

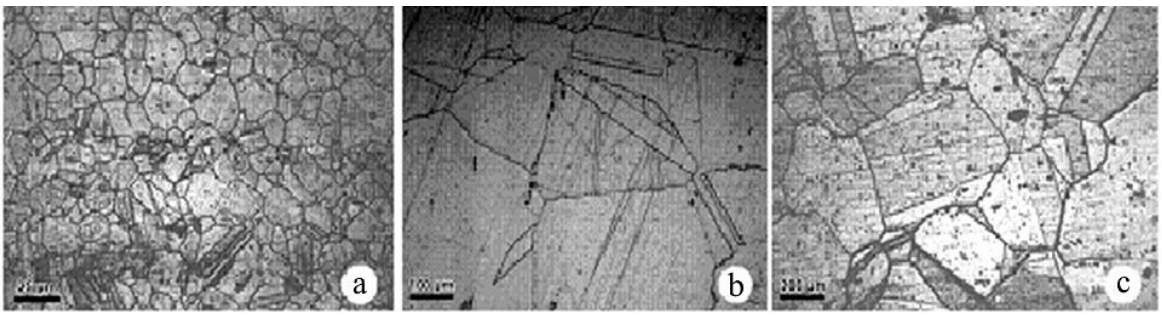

Fig. 1. Microstructure of a KhN43MBTYu alloy (CCI) after HTI (a), HTII (b), HTIII (c).

The structural characteristics of the investigated alloy modifications, hydrogen content absorbed as a result of preholding at 623 K, 35 MPa for 10 h and mechanical properties, at room temperature and an extension rate of 0.1 mm/min, of specimens hydrogen-uncharged in air and hydrogen-precharged in hydrogen at a pressure of 35 MPa are listed in Table 3.

The strength and ductility characteristics were determined on standard 25 mm long cylindrical specimens with a test portion diameter of 5 mm. The tensile tests were carried out according to GOST 9651-84 (ISO 783-89) [15], and the fracture toughness was determined according to GOST 25506-85 [16]. The stress intensity factor under static load, K_Q, was calculated according to the standard [17] under eccentric extension at a rate of 0.1 mm/min in air and 0.01–100 mm/min in hydrogen. Since the strain rate of 0.1 mm/min does not correspond to the range specified in GOST 9651-84 (1.2–12 mm/min), some tests were carried out at a rate of 5 mm/min. The results obtained at different rates in the air did not differ. The effect of the specimen thickness on the fracture behavior in hydrogen and air was studied on $10 \times 24 \times 25$, $13 \times 31 \times 33$, $15 \times 36 \times 38$, $20 \times 48 \times 50$, and $25 \times 60 \times 62$ mm rectangular compact specimens. The length of pre-induced fatigue crack $l = (0.45–0.55)b$, where b is the specimen width.

To correctly determine K_{Ic}, a number of plane strain (PS) conditions must be ensured in the specimen [1, 3, 14, 16], which is impossible for high-ductility materials without significantly increasing its size and using super-powerful equipment. Therefore, the fracture toughness under elastic-plastic fracture conditions was determined by the J-integral method [17] on specimens with a fatigue pre-crack of relative length $\varepsilon = l/b = 0.5$, providing in this case the relation $K_{max} \le 0.6K_{Ic}$. The thickness of specimens was 20 mm, the extension rate was 0.1 mm/min. The critical SIF $K_{Ic}(J)$ under plane strain conditions was determined from the J_{Ic} value using the relation $K_{Jc}^2 = J_{Ic}E/(1-\mu^2)$, where E is elastic modulus, and μ is Poisson's ratio.

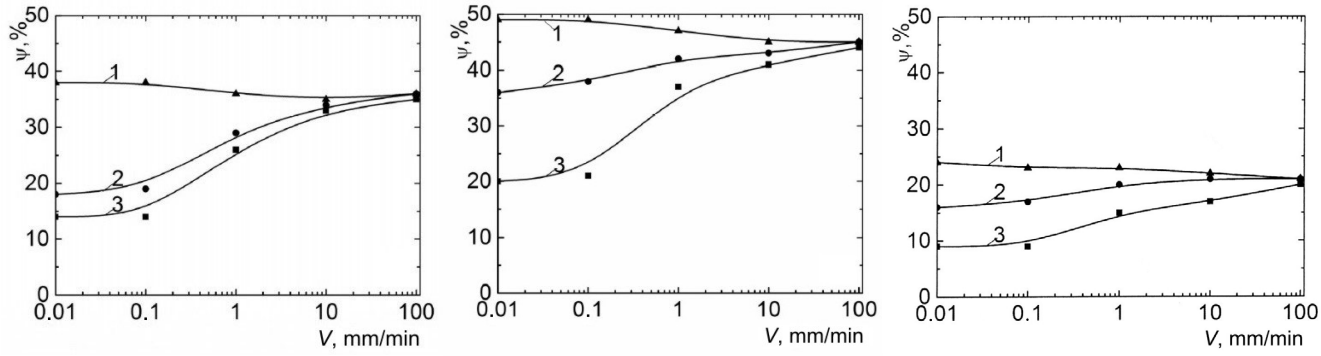

Fig. 2. Dependence of the lateral contraction ratio of KhN43MBTYu alloy specimens in helium (*1*), in hydrogen under a pressure of 35 MPa (*2*), and in hydrogen under a pressure of 35 MPa after hydrogen precharging (mode 1) (*3*) on the extension rate: (a) CCI, HTI; (b) CCII, HTI; (c) CCII, HTIII.

Crack growth under long-term static load was studied, using a loading scheme with constant opening displacement, on $150 \times 24 \times 12$ mm double cantilever beam (DCB) specimens with fatigue cracks of average length 30 mm by the procedure [18]. During the research, the length of the crack and its extension on both specimen sides were determined visually with a BMI-1 toolmaker's microscope (readability 0.001 mm) to construct a plot of the time variation of its length, and the growth rate V was determined. The mean value of the length on both specimen sides was used, the difference between which was not over 10%. Hydrogen-precharged specimens (hydrogen content $C_{\mathrm{H}} = 18$ ppm) were held in hydrogen at a pressure of 35 MPa. Symmetrical 60° edge 1.5mm-deep V-notches facilitate the formation of PS conditions in the specimen and guide the crack propagation ditrection [18]. The predetermined maximum fatigue test duration reached 300 h.

To simulate the influence of hydrogen absorbed because of the long operation of products in hydrogen-containing environments, some of the specimens were preliminarily held in working chambers at 623 K and a hydrogen pressure of 35 MPa for 10 h (mode 1) and 30 h (mode 2). After hydrogen charging and tests, the specimens were cooled to cryogenic temperature, and after 15–20 h, the hydrogen content of them was determined with a Leco TCH-600 device. The hydrogen-charged and uncharged specimens were tested in the air and hydrogen at a pressure of 35 MPa at room temperature. The hydrogen degradation susceptibility was assessed from the coefficient β, which was determined as the ratio of the values of relevant characteristics in hydrogen and air.

Results and Discussion. *Effect of Chemical Composition, Heat Treatment Modes, and Deformation Rate on the Ductility and Fracture Toughness Characteristics.* The mechanical properties of steels and alloys in hydrogen depend on the loading rate [1–3, 7–12]. At a constant hydrogen pressure, the embrittlement rate range and the degree of maximum embrittlement are determined by the chemical composition and structural state of the material.

Under the action of hydrogen, there occurs a reduction in the short-term strength (of up to 20%), elongation (by a factor of 7), lateral contraction ratio and fracture toughness (by a factor of up to 2.5) of the alloy (Table 3). Since the alloy in the hardened state is only slightly sensitive to hydrogen (Table 3), the dependencies of mechanical characteristics on the loading rate were studied on specimens after aging. At room temperature, the ductility characteristics of all modifications do not almost change with increasing static extension rate in the air (curves *1* in Fig. 2) and greatly increase in hydrogen (curves *2* and *3*). The maximum hydrogen embrittlement occurs in a loading rate range of 0.01–0.1 mm/min, i.e., as in the range determined earlier [10, 11] in 10Kh11N23T3MR and 10Kh15N27T3MR precipitation-hardening austenitic steels. Unlike the above steels, structural carbon [19], and stainless austenitic and martensitic [1, 2, 6–11, 20, 21] steels, not the lateral contraction ratio ψ, but the relative elongation δ is a more hydrogen-sensitive characteristic of the KhN43MBTYu alloy (they decrease maximally by a factor of 2.7 and 7 respectively) (Table 3). This peculiarity of the influence of gaseous hydrogen is also typical of nickel alloys [1, 2, 6, 8, 10, 14, 20, 21], indicating the localization of deformation of specimens during loading.

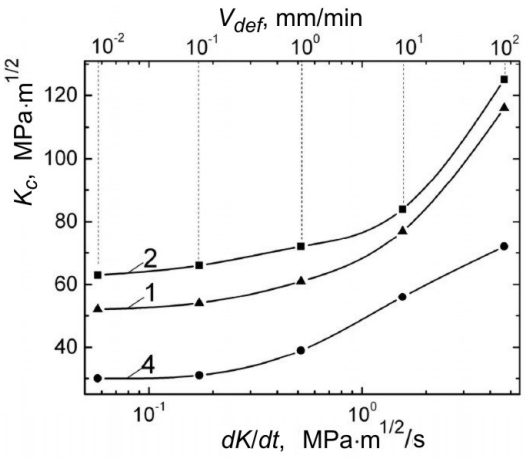

Fig. 3. Effect of the rate of variation of SIF dK/dt (extension rate V_{def}), on the fracture toughness, under a hydrogen pressure of 35 MPa, of hydrogen-charged (mode 1) KhN43MBTYu alloy specimens with a thickness of 20 mm (*1*, *2*, *4* = Nos. in Table 2).

The lowest hydrogen embrittlement resistance is observed in alloy specimens with CCII after HTIII (Tables 1–3) with coarse-grained structure and the largest amount of the γ' phase (14 wt.%) and carbides (1.0 wt.%), and with the average bulk concentration of hydrogen $C_{\mathrm{H}} = 18$ ppm (Fig. 2c, curve *4* in Fig. 3). Heat treatment, which simulates soldering (No. 3 in Table 2), causes a significant grain growth to 190 μm (Fig. 1b), formation of a nickel- and iron-based gamma solid solution, a reduction in the percentage of the γ' phase (6 wt.%) and carbides (0.5 wt.%) and, as a consequence, a significant decrease in the strength and fracture toughness characteristics K_{Jc} and K_c in air. With this chemical composition and this structure, the strength, ductility and fracture toughness parameters do not practically change in hydrogen, i.e., the alloy is slightly sensitive to hydrogen embrittlement (No 3 in Table 3). The highest fracture toughness K_{Jc}, K_c and mechanical properties in air have been obtained for the alloy with CCII after HTI (No. 2 in Table 2, Fig. 1b, curve *2* in Fig. 3). The reduction in the carbon and sulfur content of the alloy after hardening and two-stage aging provided a higher hydrogen embrittlement resistance than the alloy modifications with CCI. In this case, a fine-grained structure with γ' phase particles more uniformly distributed throughout the grain bode, a smaller amount of carbides, and the absence of their continuous chains along the grain boundaries has been obtained.

The influence of preabsorbed hydrogen is significant in the entire rate (V) range (curves *2* and *3* in Fig. 2). The hydrogen content of alloy modifications after aging and hydrogen precharging (mode 1) differs only slightly (18–21 ppm), and the smallest amount of hydrogen was found in hardened specimens (13 ppm) (CCII, HTI) (Table 3).

The dependence of the fracture toughness parameter K_c on the loading rate in hydrogen is analogous. At $dK/dt = 0.1$ MPa $\cdot$ m$^{1/2}$, its minimum value is determined by the structural state of the material (Fig. 3). The coefficients β_ψ and β_{Kc} are almost the same (Fig. 3), i.e., the hydrogen embrittlement sensitivity of SIF K_c is the same as that of the lateral contraction ratio ψ.

Thus, the formation of a structure with thin grain boundaries and the reduction in the amount of carbides increase the fracture toughness and hydrogen resistance of the alloy and do not practically affect its strength in a neutral environment.

Effect of Hydrogen Pressure and Content, and Specimen Thickness on Fracture Toughness. Earlier [6, 10, 11], it was shown that after reaching the hydrogen degradation limit of martensitic steels and highly doped nickel-chromium alloys, the ductility and low-cycle life characteristics do not deteriorate with further increase in preabsorbed hydrogen pressure and content. Such minimum values of δ and ψ [20], and K_c were found only for the more hydrogen-sensitive structural state of the KhN43MBTYu alloy after HTIII with coarse-grained structure and a large amount (of up to wt%) of the strengthening γ' phase (curve 5 in Fig. 4). It is known that hydrogen brittleness in 10Kh11N23T3MR and 10Kh15N27T3MR austenitic precipitation-hardening steels is maximal only at a significant

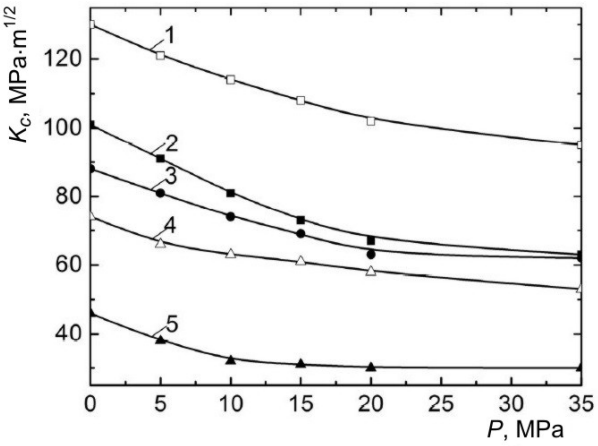

Fig. 4

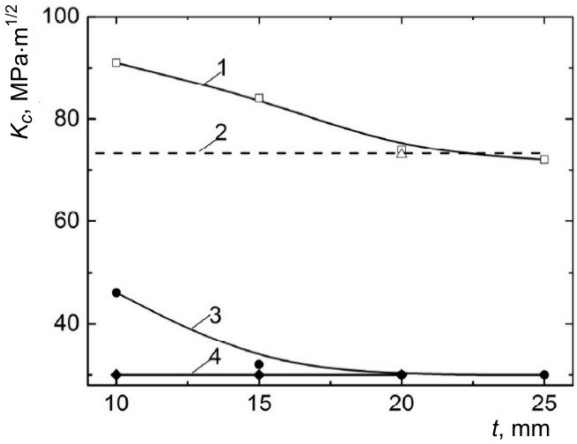

Fig. 5

Fig. 4. Effect of the hydrogen pressure P on the fracture toughness K_c of KhN43MBTYu alloy specimens (CCII) with a thickness of 20 mm after HTI (*1*–3) and HTIII (*4*, *5*): (*1*, *4*) hydrogen-uncharged specimens, (*2*, *5*) hydrogen-charged specimens (mode 1), and (*3*) hydrogen-charged specimens (mode 2).

Fig. 5. Effect of the specimen thickness t on the factor K_c of a KhN43MBTYu alloy: (*1*) air; (*2*) air, K_{Jc} values obtained by the *J*-integral method; (*3*, *4*) under a hydrogen pressure of 35 MPa at a pre-occluded hydrogen content of 18 and 29 ppm, respectively.

absorbed hydrogen content [6, 10, 11]. Therefore, some of the KhN43MBTYu alloy specimens were charged with hydrogen in mode 2 to a hydrogen content of 29 ppm, which led to an increase in the hydrogen embrittlement of the most hydrogen-resistant modification of the age-hardened alloy modifications (CCII, HTI) in the hydrogen pressure range of 0–15 MPa; at the pressure above 20 MPa, the fracture toughness decreases to minimum values of 62–63 MPa $\cdot$ m$^{1/2}$ (curve *3* in Fig. 4).

For the 20 mm thick specimens of the alloy modification with CCII and HTIII, the parameter K_c reaches the lowest value of 30 MPa $\cdot$ m$^{1/2}$ at a hydrogen content of 18 ppm and for the 10 mm thick specimens, at a hydrogen content of 29 ppm. At these conditions, the load–displacement diagrams correspond to type I according to GOST 9651-84 [16], there are no lateral contractions, and the fracture surface of specimens is covered with cleavage facets typical of brittle fracture. In this case, K_c reaches critical values K_{Ic}, i.e., corresponds to the requirements $l,\ t \geq 2.5(K_c^{\mathrm{H}}/\sigma_{0.2}^{\mathrm{H}})^2$ [5, 16, 18], where l is the crack length and t is the specimen thickness. Thus, hydrogen initiates fracture by a normal fracture mechanism along the entire crack front and causes a plane strain state (PSS).

With increasing the thickness of a compact specimen from 10 to 25 mm, the K_c values of the alloy in air decrease over the entire range studied (curve *1* in Fig. 5). At the maximum specimen thickness of 25 mm, we have $K_c = K_{Jc}$ (curves *1* and *2* in Fig. 5), and there is a flat brittle fracture surface without lateral contraction, which agrees with the known comparative results of determining fracture toughness by different experimental methods [1, 3–5, 14, 16, 18]. At the maximum hydrogen brittleness, the parameter K_c is almost independent of the specimen thickness (curve *4* in Fig. 5). Obviously, the values of the crack resistance factor K_{IcH} are critical for the alloy in the presence of hydrogen.

Some increase in the hydrogen brittleness of the alloy at the concentration $C_{\mathrm{H}} = 29$ ppm and the specimen thickness of 10–20 mm is due to the fact that at these conditions, the minimum K_c value has not been obtained (curve *1* in Fig. 6). Since depending on the specimen thickness and hydrogen content, the effect hydrogen on the parameter K_c can be noticeably stronger or weaker than that on K_{Ic} (curves *3* and *4* in Fig. 6), to correctly assess the crack resistance of materials in hydrogen-containing environments, it is important to determine the pressure or concentration of hydrogen at which the PSS occurs.

Thus, under the action of hydrogen, the fracture toughness decreases by a factor of 2.5, and the PSS occurs at a much smaller specimen thickness (Fig. 5). Hydrogen has an especially great effect on the plastic zone size, which

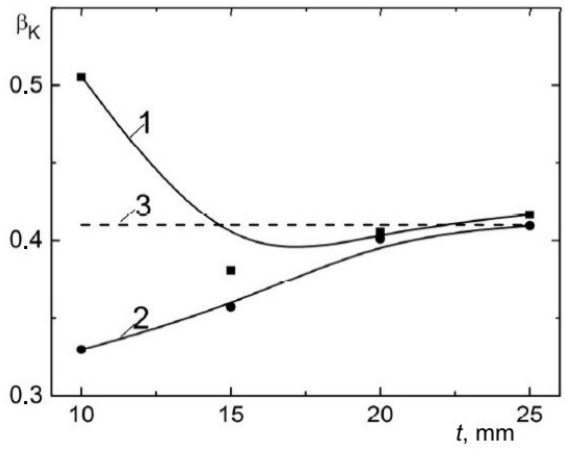

Fig. 6

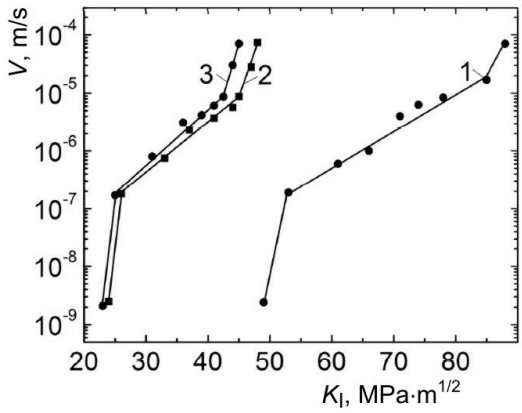

Fig. 7

Fig. 6. Dependence of the coefficient of influence of hydrogen under a pressure of 35 MPa, β_K, on K_c of a KhN43MBTYu alloy (CCII, HTII) at a pre-occluded hydrogen content of 18 (*1*) and 29 ppm (*2*) and the ratio $K_{\mathrm{IcH}}/K_{\mathrm{I}c}$ (*3*) on the specimen thickness *t*.

Fig. 7. Kinetic diagrams of hydrogen cracking of double cantilever beam specimens with a thickness of 12 mm in hydrogen at a pressure of 35 MPa (*3*) and a pre-occluded hydrogen content of 18 (*1*) and 29 ppm (*2*): (*1*) CCII, HTI, (*2*, *3*) CCII, HTIII.

is proportional to the square of the factor K_c [4, 5, 14, 18] and determines the elastic and plastic strain distribution ahead of the crack tip, fracture mode, and remaining service life. It is known that on large specimens, the plastic zone size is small compared with the crack length, residual cross section, and specimen thickness [5, 16, 18, 21, 22–30]. The embrittlement of specimens with smaller thickness and the higher ratio of the plastic zone size to the thickness is greater, but this requires higher hydrogen concentrations (Figs. 5 and 6). Thus, at the amount of hydrogen sufficient for the maximum embrittlement, its effect on fracture toughness in the plane stress state is greater than in the plane strain state.

Long-term static crack resistance of the KhN43MBTYu alloy. A peculiarity of the behavior of structural materials in the presence of hydrogen is subcritical crack growth at the SIF values much smaller than the limiting values of the parameter $K_{\mathrm{I}c}$ [5, 18, 20–30]. Then, the laws governing the hydrogen-metal interaction are evaluated, and the life of products in hydrogen-containing environments is predicted from static crack resistance diagrams, plots of the crack growth rate dl/dt versus SIF [5, 20–23].

Hydrogen-charged and uncharged specimens (Nos. 2 and 4 in Table 2) with a fatigue pre-crack were loaded to SIF values that do not exceed $K_{\mathrm{I}c}$ in air and were placed in a chamber with hydrogen under a pressure of 35 MPa. The stress intensity factor K_{I}, which corresponds to each value of deformation rate, was calculated from a known formula [25]. Because of the high hydrogen sensitivity of the alloy, it was impossible in most cases to accurately determine the threshold value $K_{\mathrm{I}HST}$; therefore, conventional SIF values $K^{V}_{\mathrm{I}HST}$, at which the crack propagation rate decreased to $5\cdot10^{-9}$ m/s, were used as a fracture toughness characteristics [25].

It has been found that the specimens not precharged with hydrogen did not crack in hydrogen under a pressure of 35 MPa at the specified predetermined maximum fatigue test duration. At a hydrogen concentration of 18 and 29 ppm, the kinetic fatigue fracture diagrams of coarse-grained alloy specimens after aging (No. 4 in Table 2) almost coincide (Fig. 7). Under the joint action of preabsorbed hydrogen and a hydrogen atmosphere with a pressure of 35 MPa, the threshold values $K_{\mathrm{I}HST}$ are 23–24 MPa $\cdot$ m$^{1/2}$, i.e., much smaller than $K_{\mathrm{I}cH} = 30$ MPa $\cdot$ m$^{1/2}$ of compact specimens (Table 3, Fig. 5). The more hydrogen-resistant alloy modification with fine-grained structure (No. 2 in Table 2) has a broader stable crack extension plateau and a higher threshold value $K_{\mathrm{I}HST}$ (48 MPa $\cdot$ m$^{1/2}$) (Fig. 7). Thus, to calculate the life and remaining service life of structural elements with crack-like defects, which

TABLE 4. Fracture Mechanisms of KhN43MBTYu Alloy Specimens (CCII) after Different Heat Treatment and under Different Test Conditions at an Extension Rate of 0.1 mm/min

Type of loading	Test conditions	Site of analysis	HTI	HTIII
Extension	Air	Center	Transgranular fracture, equiaxed dimples	Intergranular fracture, equiaxed dimples
		Taper	Transgranular fracture, parabolic dimples	Intergranular fracture, cellular relief + dimples
	Hydrogen, 35 MPa after hydrogen charging (mode 1)	Center	Intergranular fracture, dimples + cellular relief	Intergranular fracture, cellular relief
		Taper	Intergranular fracture, cellular relief	Intergranular fracture, cellular relief
K_c	Air	–	Transgranular fracture, parabolic dimples	Intergranular fracture, parabolic dimples
	Hydrogen, 35 MPa after hydrogen charging (mode 1)	–	Intergranular fracture, quasi-cleavage facets	Intergranular fracture, quasi-cleavage facets

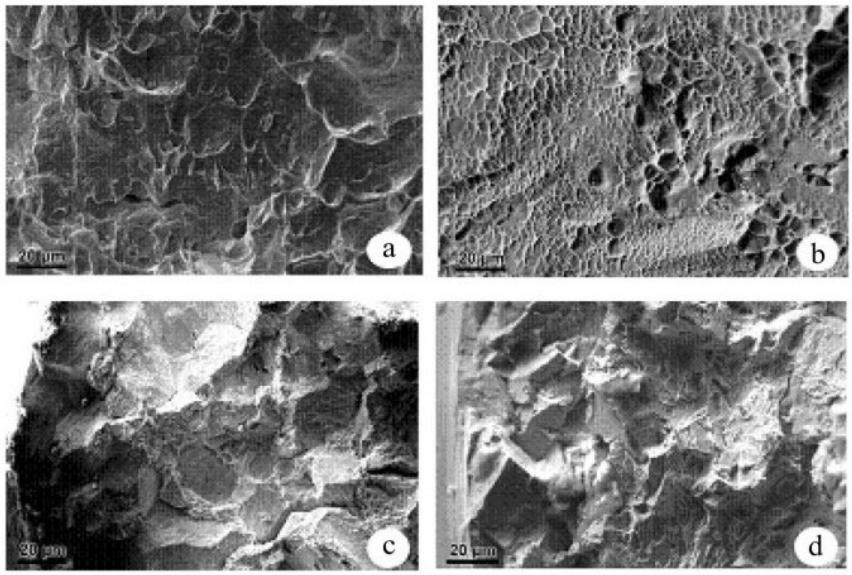

Fig. 8. Fracture micromechanisms of alloy specimens under static extension at 293 K in air (a, b) and in hydrogen at a pressure of 35 MPa after hydrogen-precharging (mode 1) (c, d): (a, c) tapered portion of the specimen; (b, d) central portion.

operate under the long-term action of gaseous hydrogen, it is more expedient to use invariant threshold SIF values K_{IHST}.

Fractographic Peculiarities of the Fracture of the Alloy in Hydrogen. Fracture mechanisms of KhN43MBTYu alloy specimens (CCII) after different heat treatment and under different test conditions at an extension rate of 0.1 mm/min are presented in Table 4. The fracture surfaces of the alloy were investigated on 25 mm long cylindrical specimens with a test portion diameter of 5 mm, subjected to static extension test. After HTI (CCI, CCII) in a vacuum, the fracture mode is ductile dimpled both on the tapered portion and in the core of the specimen, where the crack nucleates (Fig. 8).

The pattern of fracture in hydrogen depends on the strain rate. If the rate is higher than 0.1 mm/min, the fracture both in air and in hydrogen is a ductile cup-cone fracture. As the strain rate in hydrogen decreases, surface shear cracks appear on the tapered portion of the specimen, and an intergranular fracture occurs (Fig. 8c); in the core

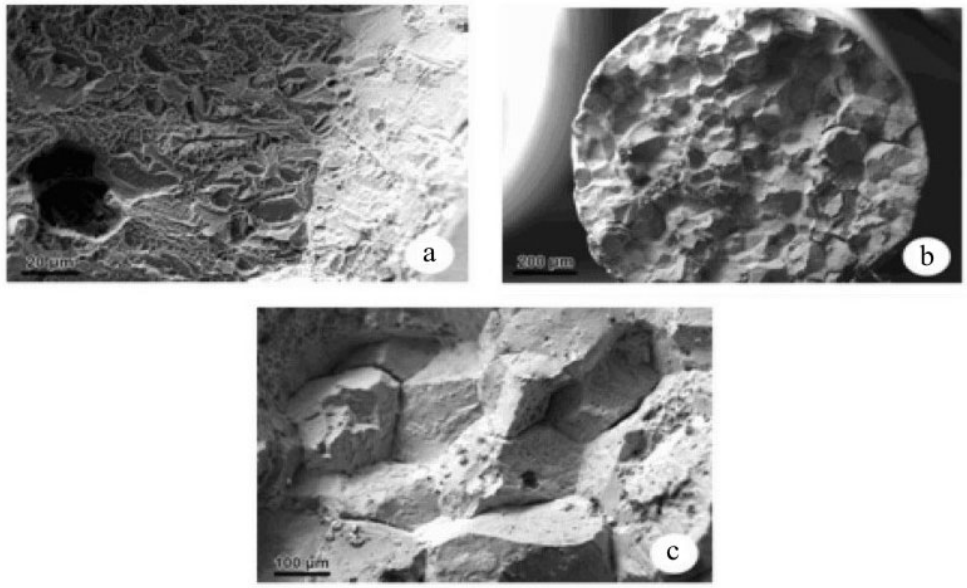

Fig. 9. Fracture of KhN43MBTYu alloy specimens under static extension in air (a) and in hydrogen at a pressure of 35 MPa after hydrogen-precharging (mode 1) (b, c): (a, c) tapered portion of the specimen; (b) macrofracture.

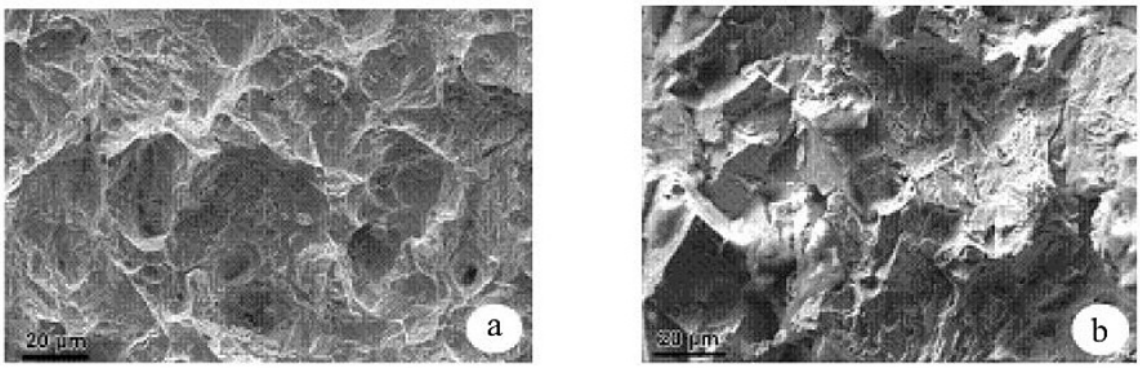

Fig. 10. Static fracture of a KhN43MBTYu alloy (CCII, HTI) near the initial fatigue crack front in air (a) and in hydrogen (b) at a pressure of 35 MPa after hydrogen-precharging (mode 1).

of the specimen, a small ductile cleavage fracture area persists (Fig. 8d). On the bottom of the cup (in air and at a strain rate of over 0.1 mm/min, in hydrogen), equiaxed dimples predominate. The tapered portion is characterized by shear dimples and smooth areas with cellular relief.

In the microstructure of the fractures of specimens tested in hydrogen at a strain rate of ≤ 0.1 mm/min, elements of different nature predominate at the sites of surface cracks: shear dimples (Fig. 8c) and areas with cellular relief (Fig. 9b). Areas with hydrogen-initiated intense secondary cracks, partly along the grain boundaries (Fig. 9b, c), appear in fractures, which is also typical of many martensitic and austenitic steels [1–7, 10–12, 14, 27–31]. The alloy specimens with coarse-grained structure fractured by cleavage independent of HT mode (HTII, HTIII) or the test environment (Fig. 9). Fracture microstructure – ductile, mainly intergranular, fracture (Fig. 9b, c). This is due to the precipitation of carbides along the grain boundaries and the formation of a large amount of the intermetallic γ' phase after additional aging (Table 3).

The fractographic investigations of the fractures of compact alloy specimens (CCII, HTI, HTIII, Table 2) were carried out on compact rectangular specimens with a thickness of 20 mm. After standard HTI (CCI, CCII) in air, the fracture mode is ductile with a dimpled microrelief inherent in ductile materials, transgranular crack propagation, and individual intergranular cracks (Fig. 10a). On the fracture surface of hydrogen-precharged

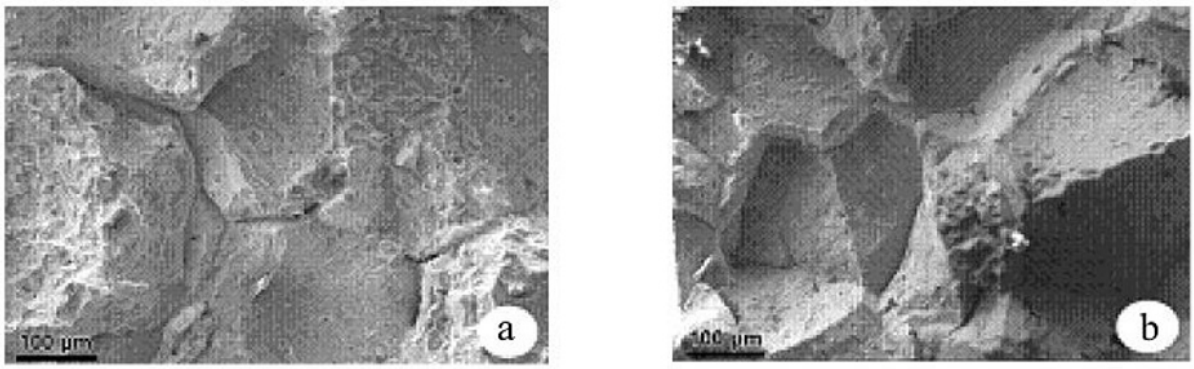

Fig. 11. Static fracture of a KhN43MBTYu alloy (CCII, HTIII) near the initial fatigue crack front in air (a) and in hydrogen (b) at a pressure of 35 MPa after hydrogen-precharging (mode 1).

specimens, intergranular fracture areas, quasi-cleavage facets with cleavage ridges along the carbide/matrix and intermetallic/matrix interfaces, and splitting in slip bands to form two- and three-dimensional facets predominate (Fig. 10b). In the fracture of alloy specimens (CCII, HTIII), the predominant microrelief feature is intergranular failure independent of the test environment (Fig. 11a, b) [24–31]. In all cases, crack nucleation and propagation in the presence of hydrogen are facilitated by structural defects, which is characteristic of the hydrogen embrittlement of steels and alloys [1–12, 14, 19–21, 24–30].

CONCLUSIONS

1. The stress intensity factor in the presence of hydrogen, just as the ductility characteristics of smooth specimens, depends largely on the loading rate. The level of K_c ddrops with a decrease in dK/dt (V_{def}) to the minimum value, which is determined by the chemical composition and structure of the material.

2. The formation of a structure with thin grain boundaries and reduction in the amount of carbides increase the fracture toughness and hydrogen resistance of the alloy and do not practically affect its strength in a neutral environment.

3. Under the action of hydrogen, the fracture toughness drops by a factor of 2.5, and the PSS occurs in specimens of much smaller thickness. Hydrogen has an especially strong effect on the plastic zone size, which is proportional to the square of the factor K_c and which determines the elastic and plastic strain distribution ahead of the crack tip, fracture mode, and residual service life.

4. In long-term static crack resistance tests at the predetermined maximum fatigue test duration of 300 h, the invariant crack resistance characteristics – the threshold values K_{1HST} of 23–24 and 48 MPa $\cdot$ m$^{1/2}$ – were determined for different alloy modifications with low carbon and chromium content.

5. Hydrogen causes a reduction in the size of dimples and an increase in the percentage of cleavage planes and intergranular fracture areas in fractures. This indicates a strain localization, the intensification of normal and shear fracture, and a reduction in intergranular cohesion.

REFERENCES

1. J. A. Lee, “Hydrogen embrittlement of nickel, cobalt and iron-based superalloys,” in: R. P. Gangloff and B. P. Somerday (Eds.), *Gaseous Hydrogen Embrittlement of Materials in Energy Technologies*, Vol. 1: *The Problem, Its Characterization and Effects on Particular Alloy Classes*, Woodhead Publishing (2012), pp. 624–667.
2. M. Dadfarnia, A. Nagao, S. Wang, et. al., ”Recent advances on hydrogen embrittlement of structural materials,” *Int. J. Fracture*, **196**, 223–243 (2015).

3. A. M. Syrotyuk and I. M. Dmytrakh, "Methods for the evaluation of fracture and strength of pipeline steels and structures under the action of working media. Part I. Influence of the corrosion factor," *Mater. Sci.*, **50**, No. 3, 324–339 (2014).
4. A. I. Balitskii and V. V. Panasyuk, "Workability assessment of structural steels of power plant units in hydrogen environments," *Strength Mater*., **41**, No. 1, 52–57 (2009).
5. A. M. Syrotyuk and I. M. Dmytrakh, "Methods for the evaluation of fracture and strength of pipeline steels and structures under the action of working media. Part II. Influence of hydrogen-containing media," *Mater. Sci.*, **50**, No. 4, 475–487 (2015).
6. A. I. Balitskii, V. I. Vytvytskyi, and L. M. Ivaskevich, "The low-cycle fatigue of corrosion-resistant steels in high pressure hydrogen," *Procedia Engineer*., **2**, No. 1, 2367–2371 (2010).
7. O. Barrera, D. Bombac, Y. Chen, et al., "Understanding and mitigating hydrogen embrittlement of steels: a review of experimental, modelling and design progress from atomistic to continuum," *J. Mater. Sci.*, **53**, 6251–6290 (2018).
8. D. M. Symons, "A comparison of internal hydrogen embrittlement and hydrogen environment embrittlement of X-750," *Eng. Fract. Mech.*, **68**, 751–771 (2001).
9. D. Delafosse, X. Feaugas, I. Aubert, et al., "Hydrogen effects on the plasticity of FCC nickel and austenitic alloys," in: B. Somerday, P. Sofronis, and R. Jones (Eds.), *Effects of Hydrogen on Materials* (Proc. of the 2008 Int. Hydrogen Conf., Sept. 7–10, 2008, WY, USA), ASM International, Material Park, OH (2009), pp. 78–87.
10. A. I. Balitskii and L. M. Ivaskevich, "Assessment of hydrogen embrittlement in high-alloy chromium-nickel steels and alloys in hydrogen at high pressures and temperatures," *Strength Mater.*, **50**, No. 6, 880–887 (2018).
11. A. Balitskii, L. Ivaskevich, V. Mochulskyi, et al., "Influence of high pressure and high temperature hydrogen on fracture toughness of Ni-containing steels and alloys," *Arch. Mech. Eng*., **61**, No. 1, 129–138 (2014).
12. N. A. Sorokina, T. K. Sergeeva, Yu. I. Rusinovich et al., "Hydrogen embrittlement resistance of differently doped nickel alloys," *Fiz.-Khim. Mekh. Mater*., **21**, No. 1, 27–31 (1985).
13. C. T. Sims, N. S. Stoloff, and W. C. Hagel (Eds.), *Superalloys II*, Wiley, New York (1987).
14. O. I. Balyts'kyi, V. M. Mochyl'skyi, and L. M. Ivas'kevych, "Evaluation of the influence of hydrogen on mechanical characteristics of complexly alloyed nickel alloys," *Mater. Sci.*, **51**, No. 4, 538–547 (2016).
15. *GOST 9651-84. Metals. Methods of Elevated-Temperature Tensile Testing* [in Russian], Publishing House of Standards, Moscow (1984).
16. *GOST 25506-85. Methods for the Mechanical Testing of Metals. Determination of Crack Resistance (Fracture Toughness) Characteristics under Static Loading* [in Russian], Publishing House of Standards, Moscow (1985).
17. *ASTM E1820-08. Standart Test Method for Measurement of Fracture Toughness*, ASTM International, West Conshohocken, PA (2008).
18. M. O. Speidel and M. V. Hyatt, *Stress-Corrosion Cracking of High-Strength Aluminum Alloys*, in: M. G. Fontana and R. W. Staehle (Eds.), *Advances in Corrosion Science and Technology*, Vol. 2, Springer, Boston, MA (1972), pp. 115–335.
19. O. Z. Student, A. D. Markov, and H. M. Nykyforchyn, "Specific features of the influence of hydrogen on the properties and mechanism of fracture of the metal of welded joints of steam pipelines at thermal power plants," *Mater. Sci.*, **42**, No. 4, 451–460 (2006).
20. A. Balitskii, V. Vytvytskyii, I. Ivaskevich, and J. Eliasz, "The high- and low-cycle fatigue behavior of Ni-contain steels and Ni-alloys in high pressure hydrogen," *Int. J. Fatigue*, **39**, 32–37 (2012).
21. D. Holländer, D. Kulawinski, A. Weidner, et al., "Small-scale specimen testing for fatigue life assessment of service-exposed industrial gas turbine blades," *Int. J. Fatigue*, **92**, 262–271 (2016).
22. B. A. Kolachev, *Hydrogen Brittleness of Metals* [in Russian], Metallurgiya, Moscow (1985).
23. O. N. Romaniv and G. N. Nikiforchin, *Corrosion Fracture Mechanics of Structural Alloys* [in Russian], Metallurgiya, Moscow (1986).

24. I. Dmytrakh, “Corrosion fracture of structural metallic materials: Effect of electrochemical conditions in crack,” *Strain. Int. J. Exp. Mech*., **47**, 427–435 (2011).
25. W. F. Brown and J. E. Srawley, *Plane Strain Crack Toughness Testing of High Strength Metallic Materials*, ASTM STP 410, ASTM International, West Conshohocken, PA (1966).
26. M. H. Stashchuk, “Influence of hydrogen concentration on the stresses in a solid metallic cylinder,” *Mater. Sci.*, **53**, No. 6, 823–831 (2018).
27. P. V. Yasniy, I. B. Okipnyi, P. O. Maruschak, et al., “Crack tip strain localization on mechanics of fracture of heat resistance steel after hydrogenation,” *Theor. Appl. Fract. Mech.*, **63–64**, 63–68 (2013).
28. P. V. Yasniy, I. B. Okipnyi, P. O. Maruschak, et al., “Toughness and failure of heat resistance steel before and after hydrogenation,” *Theor. Appl. Fract. Mech*., **56**, 63–67 (2011).
29. V. I. Tkachov, L. M. Ivas’kevych, and V. M. Mochul’skyi, “Temperature dependences of the mechanical properties of austenitic and martensitic steels in hydrogen,” *Mater. Sci.*, **43**, No. 5, 654–666 (2007).
30. O. I. Balyts’kyi, L. M. Ivas’kevych, and V. M. Mochul’s’kyi, “Mechanical properties of martensitic steels in gaseous hydrogen,” *Strength Mater.*, **44**, No. 1, 64–71 (2012).
31. O. I. Balyts’kyi and O. O. Krokhmal’nyi, “Pitting corrosion of 12Kh18AG18Sh steel in chloride solutions,” *Mater. Sci.*, **35**, No. 3, 389–394 (1999).